Supplementary Information

Pyruvate MID measurements dramatically improve precision of PK flux estimates

A previous ^{13}C flux analysis of SA590 (−thiamin) reported low PK flux and diversion of PEP into a three-step bypass pathway involving the enzymes PEP carboxylase (PEPC), malate dehydrogenase (MDH), and malic enzyme (ME) (Jazmin et al., 2017). However, Jazmin et al. were unable to detect pyruvate MIDs by GC-MS analysis of MOX-TMS derivatives. Since pyruvate is the product of PK, we hypothesized that direct measurement of pyruvate MIDs would improve our ability to accurately estimate PK flux. To address this issue, we performed ^{13}C flux analysis of SA590 (+thiamin) based on GC-MS of MOX-TBDMS derivatives, which provide reproducible pyruvate MID measurements through assessment of the PYR174 fragment ion (**Fig. S6**). Although the derivatization method and experimental conditions (+/− thiamin, as well as light intensity and culture volume) were different, the flux estimates obtained from the two studies were largely consistent (**Fig. S7**). There were significant differences in flux estimates from 3PGA to pyruvate and from pyruvate to IBA, as expected due to differences in IBA productivity of the two cultures. Significantly, the SA590 (+thiamin) study determined a high PK flux estimate, while the SA590 (−thiamin) study determined a low PK flux and high flux through the three-step PK bypass pathway (PPC → MDH → ME). Flux to IBA (via the ALS reaction) was approximately doubled in the SA590 (+thiamin) condition, which was also associated with increased enolase (ENO) flux from 3PGA to PEP.

To further test the sensitivity of each best-fit solution to variations in PK flux, we constrained the PK flux to zero in the INST-MFA model and regressed both the MOX-TBDMS measurements (from SA590, +thiamin) and the prior MOX-TMS measurements (from SA590, −thiamin) to determine whether the adjusted model could still achieve an acceptable fit. We assessed the lack-of-fit between the simulated and experimentally measured MIDs by calculating the sum of squared residuals (SSR) for each best-fit solution. Constraining the INST-MFA model to a low PK flux solution while regressing the MOX-TBDMS measurements increased the SSR beyond the upper limit of the acceptable range (**Fig. S8A**). The PYR174 and MAL419 MID measurements were the major contributors to the overall lack-of-fit (**Fig. S8B**). MOX-TMS measurements, on the other hand, were not as sensitive to variations in PK flux (**Fig. S8C**), and the SSR remained within the acceptable range for both high and low PK flux solutions (**Fig. S8A**).

In summary, we found that the MOX-TBDMS measurements used in our current study are more sensitive to variations in PK flux than the MOX-TMS measurements used in our prior study, largely because the MOX-TBDMS derivatives enable accurate assessment of pyruvate MIDs. Although the two studies were conducted under different experimental conditions, the limited sensitivity to discriminate between pyruvate-producing pathways using MOX-TMS derivatives could also have contributed to the variability in PK flux estimates between the two studies. These results led us to conclude that pyruvate MID measurements are essential for precise determination of PK flux.

Table S1. Net fluxes determined by ^{13}C INST-MFA in SA590 (+thiamin), SA590-PK (−thiamin), and SA590-PK (+thiamin). Estimated flux values (µmol gDW^{-1} h^{-1}) and 95% confidence bounds are shown (n=3). The specific growth rate is specified in units of h^{-1}.

Strain (condition)		SA590 (+thiamin)			SA590-PK (−thiamin)			SA590-PK (+thiamin)		
Reaction name	*Reaction*	*Value*	*LB95*	*UB95*	*Value*	*LB95*	*UB95*	*Value*	*LB95*	*UB95*
RUBISCO_CO2	RUBP + CO2 -> 3PGA + 3PGA	1428	1314	1554	1302	1236	1392	1554	1428	1668
GAPDH	3PGA -> TP	2484	2298	2718	2256	2142	2688	2676	2460	3156
ALD	TP + E4P -> SBP	480	438	522	438	420	522	498	474	594
SBP	SBP -> S7P	480	438	522	438	420	522	498	474	594
FBA net	TP + TP <-> FBP	516	474	612	462	438	540	582	504	684
PFK net	FBP <-> F6P	516	474	612	462	438	540	582	504	684
TK1 net	TP + EC2 <-> X5P	972	894	1062	888	846	1062	1008	960	1224
TK2 net	S7P <-> R5P + EC2	480	438	522	438	420	522	498	474	594
TK3 net	F6P <-> E4P + EC2	492	444	534	450	426	534	510	480	606
PPE net	X5P <-> RU5P	972	894	1062	888	846	1062	1008	960	1224
PPI net	R5P <-> RU5P	462	426	504	426	408	510	486	462	582
PRK	RU5P -> RUBP	1434	1314	1560	1308	1242	1566	1554	1440	1854
PGI net	F6P <-> G6P	27	24	216	11	10	108	78	18	120
G6PDH	G6P -> RU5P + CO2	0	0	90	10	0	28	59	0	84
RUBISCO_O2	RUBP -> 3PGA + 2PG	2	1	72	7	0	174	2	0	210
PGP	2PG -> GLY	2	1	72	7	0	174	2	0	210
GDC	GLY + GLY -> SER + CO2	1	0	35	3	0	90	1	0	108
SGA	SER -> GA	1	0	35	3	0	90	1	0	108
GK net	GA <-> 3PGA	1	0	35	3	0	90	1	0	108
ENO net	3PGA <-> PEP	348	324	372	336	324	354	408	390	432
PK	PEP -> PYR	234	222	276	276	258	288	336	312	372
ALS	PYR + PYR -> AcLAC + CO2	66	59	66	84	78	90	132	120	138
KIV1	AcLAC -> IBA + CO2	66	59	66	84	78	90	132	120	138
PDH	PYR -> ACA + CO2	114	102	126	84	78	90	78	72	78
CS	OAA + ACA -> CIT	28	25	31	22	20	23	19	18	20
ACO net	CIT <-> ICI	28	25	31	22	20	23	19	18	20
IDH	ICI -> AKG + CO2	28	25	31	22	20	23	19	18	20
FUM net	FUM <-> MAL	16	14	17	12	11	13	11	10	11
MDH net	OAA <-> MAL	14	-17	20	-12	-13	-10	6	-11	24
ME	MAL -> PYR + CO2	30	0	37	0	0	2	17	0	35
PPC	PEP + CO2 -> OAA	90	56	96	46	43	49	57	39	72
Growth (h^{-1})	0.715*R5P + 3.624*ACA + 1.191*G6P + 0.501*E4P + 1.205*3PGA + 1.002*PEP + 1.197*PYR + 2.039*OAA + 1.233*AKG + 0.133*TP + 1.017*CO2 -> Biomass + 0.683*FUM	0.023	0.021	0.025	0.018	0.016	0.019	0.015	0.015	0.016

Table S2. Exchange fluxes determined by ^{13}C INST-MFA in SA590 (+thiamin), SA590-PK (−thiamin), and SA590-PK (+thiamin). The exchange flux is the minimum of the forward and backward fluxes of a reversible reaction. Estimated flux values are scaled according to the transformation $v_{exch}^{[0,100]} = \frac{v_{exch}}{v_{ref} + v_{exch}} \times 100$, where v_{ref} is net CO_2 assimilation rate (Wiechert and de Graaf, 1997). 95% confidence bounds are shown for each strain/condition (n=3). Note that PGM, GS, SDH, ALT, LDH, and CBS reactions allow for reversible exchange without net flux in either direction.

Strain (condition)		**SA590 (+thiamin)**			**SA590-PK (−thiamin)**			**SA590-PK (+thiamin)**		
Reaction name	*Reaction*	*Value*	*LB95*	*UB95*	*Value*	*LB95*	*UB95*	*Value*	*LB95*	*UB95*
FBA exch	TP + TP <-> FBP	0	0	100	0	0	24	0	0	100
PFK exch	FBP <-> F6P	0	0	100	100	0	100	100	0	100
TK1 exch	TP + EC2 <-> X5P	100	0	100	100	0	100	0	0	100
TK2 exch	S7P <-> R5P + EC2	95	0	100	0	0	100	100	0	100
TK3 exch	F6P <-> E4P + EC2	100	0	100	0	0	100	50	0	100
PPE exch	X5P <-> RU5P	0	0	100	0	0	100	100	0	100
PPI exch	R5P <-> RU5P	100	0	100	100	0	100	100	0	100
PGI exch	F6P <-> G6P	0	0	100	0	0	100	1	0	100
PGM exch	G6P <-> G1P	100	0	100	100	0	100	100	0	100
GS exch	G1P <-> GLYC	100	0	100	0	0	100	91	0	100
GK exch	GA <-> 3PGA	20	6	79	14	6	20	46	0	100
ENO exch	3PGA <-> PEP	70	0	100	1	0	100	100	0	100
ACO exch	CIT <-> ICI	2	1	4	5	4	6	6	3	9
SDH exch	SUC <-> FUM	100	0	100	2	1	2	8	4	11
FUM exch	FUM <-> MAL	0	0	3	1	0	3	2	0	10
MDH exch	OAA <-> MAL	-1	0	2	0	0	1	0	0	2
ALT exch	PYR <-> ALA	100	0	100	0	0	4	8	0	22
LDH exch	LAC <-> PYR	13	12	16	17	15	18	33	15	42
CBS exch	SER <-> CYST	0	0	2	0	0	9	0	0	9

Table S3. Pool sizes determined by ^{13}C INST-MFA for SA590 (+thiamin), SA590-PK (−thiamin), and SA590-PK (+thiamin). The 95% confidence bounds on the estimated pool sizes (μmol/gDW) are shown for each strain/condition (n=3). Best-fit estimates of metabolically active pool sizes (as a percentage of total pool) were obtained for 3PGA and PEP based on their MID measurements (Ma et al., 2014).

Strain (condition)	SA590 (+thiamin)			SA590-PK (−thiamin)			SA590-PK (+thiamin)		
Metabolite	*Value*	*LB95*	*UB95*	*Value*	*LB95*	*UB95*	*Value*	*LB95*	*UB95*
2PG pool	1E-04	0E+00	2E-01	1E-04	0E+00	2E-01	1E-04	0E+00	4E-01
3PGA pool	5E+00	0E+00	8E+00	9E-03	0E+00	2E+00	1E-04	0E+00	1E+01
3PGA active pool (%)	70	67	73	N/A	N/A	N/A	46	43	49
ACA pool	6E-04	0E+00	6E+00	5E-03	0E+00	2E+00	2E-04	0E+00	3E+00
AKG pool	1E-04	0E+00	∞	1E-04	0E+00	∞	1E-04	0E+00	∞
ALA pool	2E-01	0E+00	2E+00	3E-04	3E-04	2E+00	8E+07	0E+00	∞
AcLAC pool	9E+06	0E+00	∞	9E+06	0E+00	∞	9E+06	0E+00	∞
CIT pool	4E-01	0E+00	8E-01	4E-01	0E+00	7E-01	1E-04	0E+00	3E+00
CO2 pool	6E+00	0E+00	9E+00	1E-04	0E+00	2E+00	2E-04	0E+00	1E+01
CYST pool	3E-01	1E-01	2E+01	9E-01	7E-01	2E+01	4E-01	3E-01	3E+01
E4P pool	2E-03	0E+00	4E+00	1E+00	0E+00	7E+00	5E+00	0E+00	1E+01
EC2 pool	2E-03	0E+00	6E+00	6E-01	0E+00	9E+00	1E-04	0E+00	8E+00
F6P pool	2E-03	0E+00	3E+00	1E-04	0E+00	8E+00	4E-04	0E+00	7E+00
FBP pool	9E-04	0E+00	3E+00	5E+00	0E+00	8E+00	1E-04	0E+00	7E+00
FUM pool	2E+01	0E+00	3E+01	1E-04	0E+00	4E-01	1E-04	0E+00	5E+00
G1P pool	9E-02	0E+00	∞	7E-03	0E+00	6E+00	2E+01	0E+00	∞
G6P pool	5E+06	0E+00	∞	1E-02	0E+00	4E+00	3E-01	0E+00	∞
GA pool	8E+00	3E+00	1E+01	2E+01	1E+01	3E+01	1E+01	0E+00	2E+01
GLY pool	1E-04	0E+00	2E-01	1E-04	0E+00	2E-01	1E-04	0E+00	4E-01
GLYC pool	3E-02	0E+00	∞	6E+01	0E+00	∞	3E-03	0E+00	∞
IBA pool	1E+03	0E+00	∞	1E+03	0E+00	∞	1E+03	0E+00	∞
ICI pool	3E+01	1E+01	∞	5E+01	4E+01	8E+01	4E+01	2E+01	∞
LAC pool	2E+02	2E+02	4E+02	1E+02	1E+02	1E+02	2E+02	7E+01	3E+02
MAL pool	1E+00	4E-01	4E+00	2E+00	1E+00	6E+00	3E+00	4E-01	2E+02
OAA pool	1E-04	0E+00	2E-01	2E-01	0E+00	6E-01	2E+00	8E-01	4E+00
PEP pool	2E-03	0E+00	1E+01	1E-02	0E+00	2E+00	1E-04	0E+00	1E+01
PEP active pool (%)	79	75	85	77	76	79	59	55	64
PYR pool	8E-01	0E+00	2E+00	1E-04	0E+00	7E-01	6E+00	0E+00	1E+01
R5P pool	3E-04	0E+00	3E+00	1E-04	0E+00	1E+00	1E-04	0E+00	5E+00
RU5P pool	4E-04	0E+00	3E+00	1E-04	0E+00	1E+00	1E-04	0E+00	5E+00
RUBP pool	2E-04	0E+00	3E+00	1E-04	0E+00	1E+00	1E-04	0E+00	5E+00
S7P pool	1E-03	0E+00	2E+00	1E-04	0E+00	9E-01	1E-04	0E+00	3E+00
SBP pool	1E-04	0E+00	2E+00	1E-04	0E+00	7E-01	1E-04	0E+00	3E+00
SER pool	3E-03	0E+00	2E-01	1E-01	9E-02	4E+00	1E-04	0E+00	4E-01
SUC pool	2E-02	0E+00	3E+01	2E+01	1E+01	2E+01	2E+01	9E+00	3E+01
TP pool	2E-03	0E+00	6E+00	1E-04	0E+00	2E+00	1E-04	0E+00	8E+00
X5P pool	8E-04	0E+00	3E+00	1E-04	0E+00	1E+00	1E-04	0E+00	6E+00

Table S4. Sum-of-squared residuals (SSR) and their expected ranges for SA590 (+thiamin), SA590-PK (−thiamin), and SA590-PK (+thiamin). All fits were accepted based on the chi-square test.

Strain (condition)	SA590 (+thiamin)			SA590-PK (−thiamin)			SA590-PK (+thiamin)		
SSR	162.4			152.2			109.4		
Expected range	110.9	–	176.9	94.2	–	155.7	102.1	–	165.7

Table S5. Plasmids generated in this study.

Plasmid	Description
pPK-αPdhB	*lac* operon-regulated expression of pk_{7942} (SYNPCC7942_0098) and α*pdhB* antisense sequence targeted to NS3 (Cb^R)
pCX0104-LuxAB-FT	Zn^{++}-inducible expression of P_{smtA}::*luxAB::*3×FLAG targeted to NS4 (Cm^R)
pCX0104-PK	Zn^{++}-inducible expression of P_{smtA}::pk_{7942} (SYNPCC7942_0098) targeted to NS4 (Cm^R)
pCX0104-ALS	Zn^{++}-inducible expression of P_{smtA}::*alsS* (*alsS* originally from *B. subtilis*) targeted to NS4 (Cm^R)
pCX0104-PCK	Zn^{++}-inducible expression of P_{smtA}::$pckA_{E.coli}$ (EG10759) targeted to NS4 (Cm^R)
pCX0104-PCK-FT	Zn^{++}-inducible expression of P_{smtA}::*pckA::*3×FLAG targeted to NS4 (Cm^R)

Refer to *Materials and Methods* for further details.

Table S6. Relevant primers used in this study.

Primer name	Sequence (5' to 3')	Description
PK 5' *Spe*I	GCC ACT AGT TGT CAT GCA ACC CAA CGA CTT TCA G	PCR of *pk* from PCC 7942
PK 3' *Xba*I	ACT TCT AGA TTA GAC GGA AAT CGG CTG CTC GGC AG	PCR of *pk* from PCC 7942
ALS 5' *Spe*I	GCC ACT AGT TGT CAT GTT GAC AAA AGC AAC	PCR of *alsS* from pSA126 (Atsumi et al., 2009)
ALS 3' *BamH*I	ATA GGA TCC CTA GAG AGC TTT CGT TTT CAT GAG	PCR of *alsS* from pSA126 (Atsumi et al., 2009)
PCK 5' *Spe*I	GCC ACT AGT TGT CAT GCG CGT TAA CAA TGG TTT G	PCR of *pckA* from *E. coli*
PCK 3' *BamH*I	ATT GGA TCC TTA CAG TTT CGG ACC AGC CGC TAC	PCR of *pckA* from *E. coli*
PCK 3' *Kpn*I	ATT GGT ACC CAG TTT CGG ACC AGC CGC TAC	PCR of *pckA* from *E. coli*
5' Sequencing primer	TTG GCA GAC TAC CGT CTC TCC GTC	Sequencing of constructs derived from pCX0104-lLuxAB
3' Sequencing primer	GCA GCC TGC TCT CTG GGA GTT TGA C	Sequencing of constructs derived from pCX0104-lLuxAB
5' PCK sequencing primer	ACT TCG TGG CGT TTA ACC TGA C	Sequencing of *pckA* insertion into pCX0104 backbone.
5' 7942 PCR primer	TCT TGC TCT GAC GCC TTA TTC	PCR to confirm insertion of target genes in PCC 7942
3' 7942 PCR primer	ATC GTC CCA AGA TCC AGA ATG T	PCR to confirm insertion of target genes in PCC 7942
rnpB forward	TGC TTG CAG GCA CAG GTA AG	RT-qPCR of house-keeping gene *rnpB* (Huang et al., 2016)
rnpB reverse	CCT CTA GCG GTC CAT AAA CGG	RT-qPCR of house-keeping gene *rnpB* (Huang et al., 2016)
pdhB forward	TCG TCA TCG TTG AAG AAT GC	RT-qPCR of *pdhB*
pdhB reverse	GGT TTT CTA GCT TGC CGT TG	RT-qPCR of *pdhB*
pdhA forward	AAG GCC CGA CAC TGA TTG AG	RT-qPCR of *pdhA*
pdhA reverse	GAG ATC GCA AAT TCC ACC GC	RT-qPCR of *pdhA*
pdhB-F	ATGGATCCGCTGAAAGCAAACGATGGAAGC	PCR of flanking region of *pdhB* start codon
pdhB-R	GTGGATCCAGAGGTCTTTGGTGACTTTATA	PCR of flanking region of *pdhB* start codon

Restriction cut sites are underlined. Translation start and stop codons are highlighted in red.

Supplemental Figures

Fig. S1

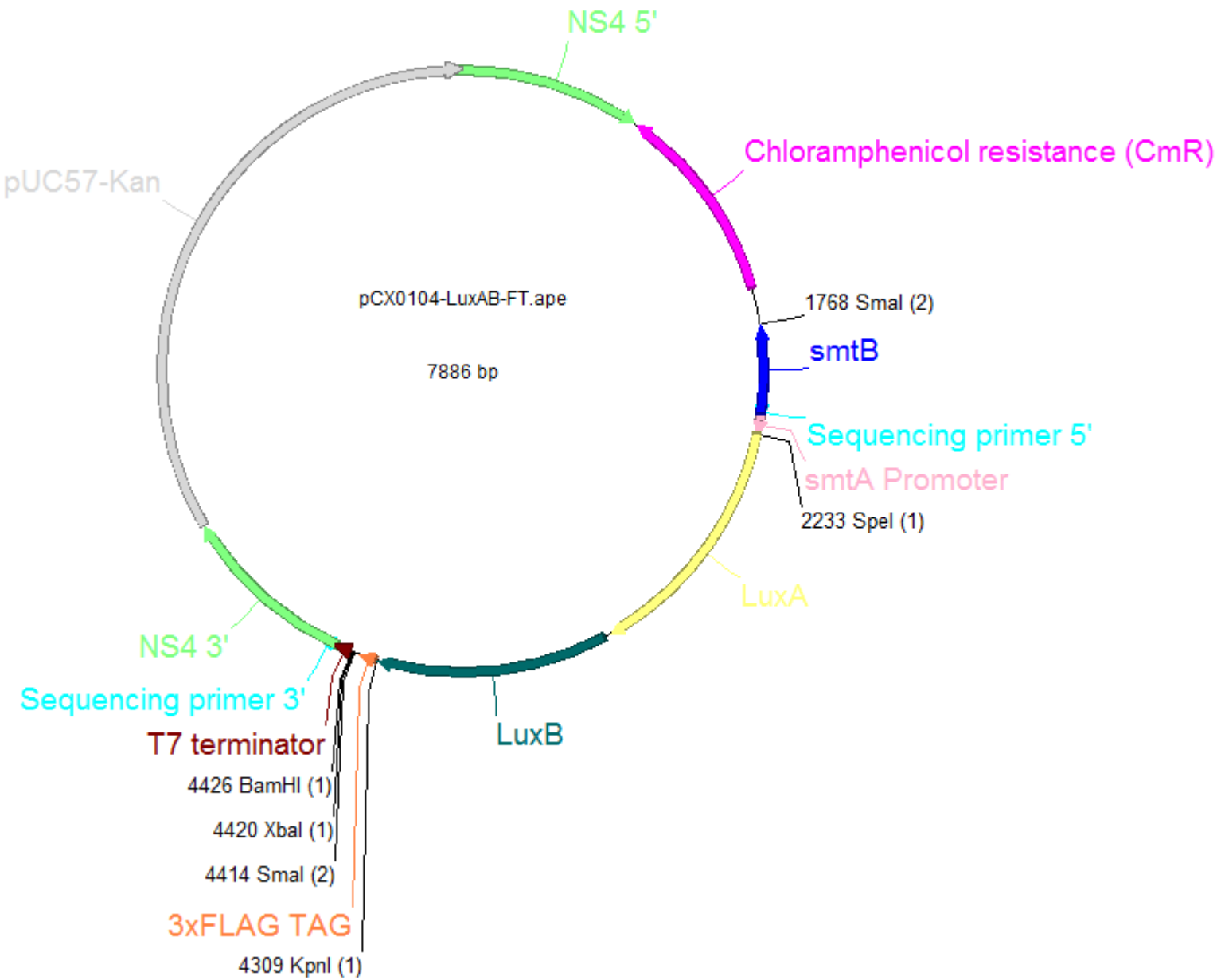
NS4 5'
Chloramphenicol resistance (CmR)
pUC57-Kan
pCX0104-LuxAB-FT.ape
7886 bp
1768 SmaI (2)
smtB
Sequencing primer 5'
smtA Promoter
2233 SpeI (1)
LuxA
NS4 3'
Sequencing primer 3'
T7 terminator
LuxB
4426 BamHI (1)
4420 XbaI (1)
4414 SmaI (2)
3xFLAG TAG
4309 KpnI (1)

Fig. S2

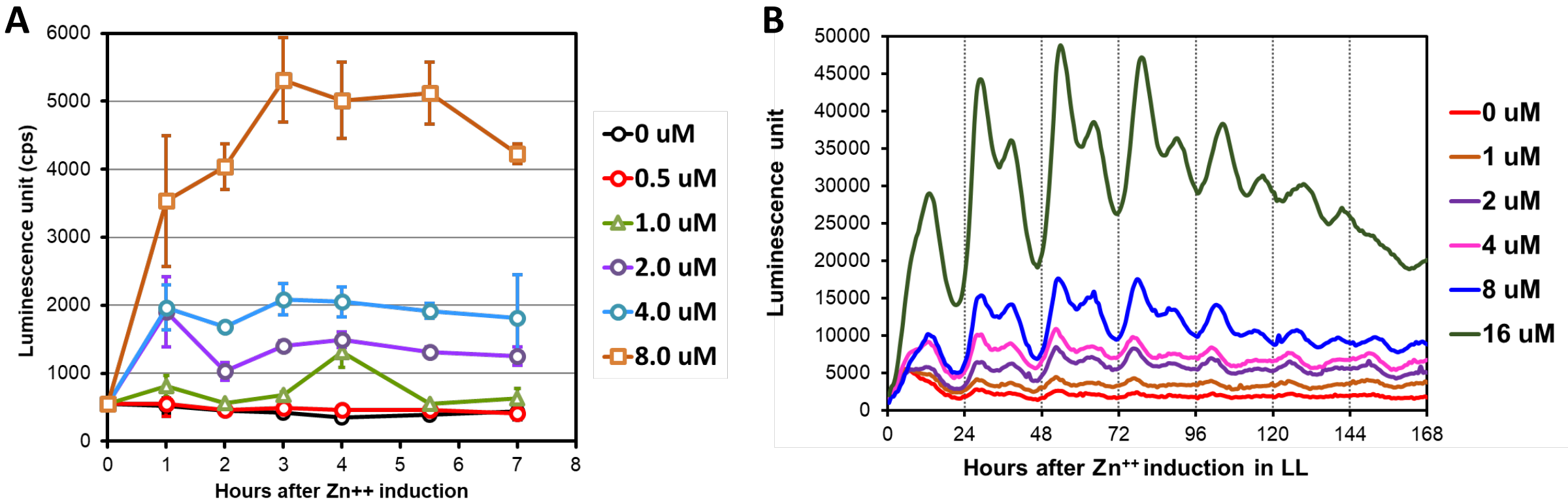
A
Luminescence unit (cps)
6000
5000
4000
3000
2000
1000
0
0
1
2
3
4
5
6
7
8
Hours after Zn++ induction
0 uM
0.5 uM
1.0 uM
2.0 uM
4.0 uM
8.0 uM
B
Luminescence unit
50000
45000
40000
35000
30000
25000
20000
15000
10000
5000
0
0
24
48
72
96
120
144
168
Hours after Zn++ induction in LL
0 uM
1 uM
2 uM
4 uM
8 uM
16 uM

Fig. S3

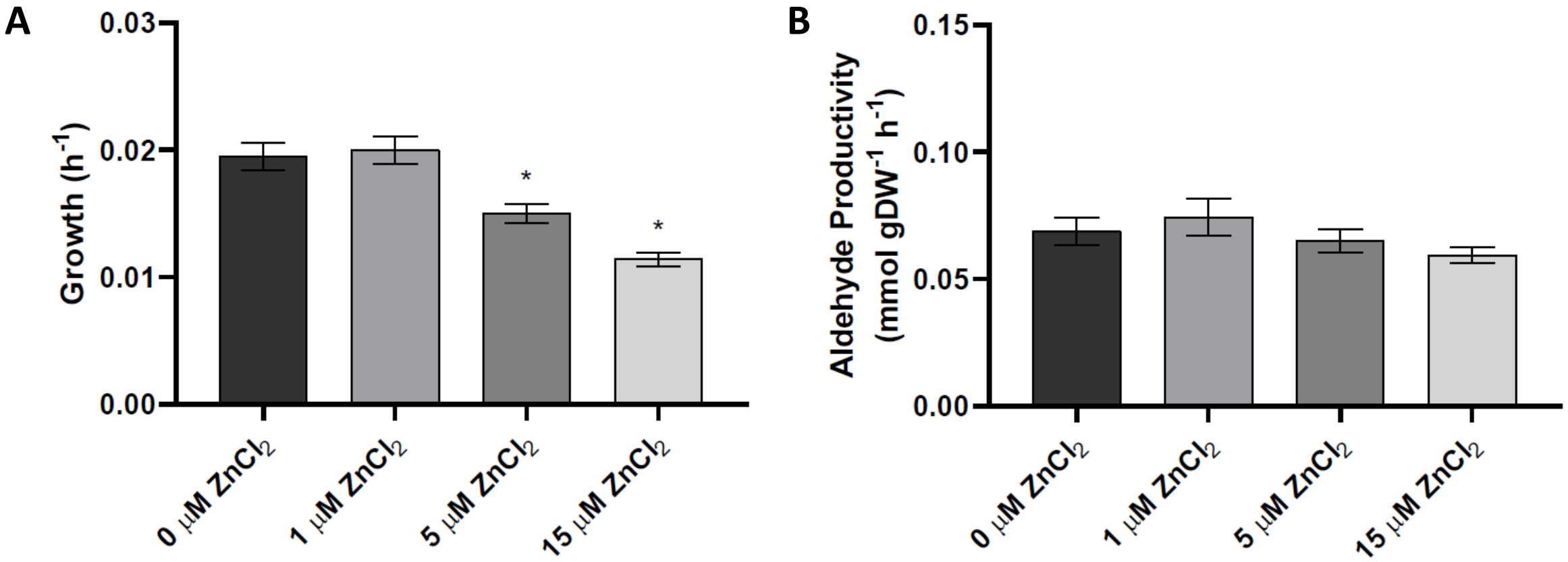
A
Growth (h^{-1})
0.03
0.02
0.01
0.00
*
*
0 μM $ZnCl_2$
1 μM $ZnCl_2$
5 μM $ZnCl_2$
15 μM $ZnCl_2$
B
Aldehyde Productivity (mmol gDW^{-1} h^{-1})
0.15
0.10
0.05
0.00
0 μM $ZnCl_2$
1 μM $ZnCl_2$
5 μM $ZnCl_2$
15 μM $ZnCl_2$

Fig. S4

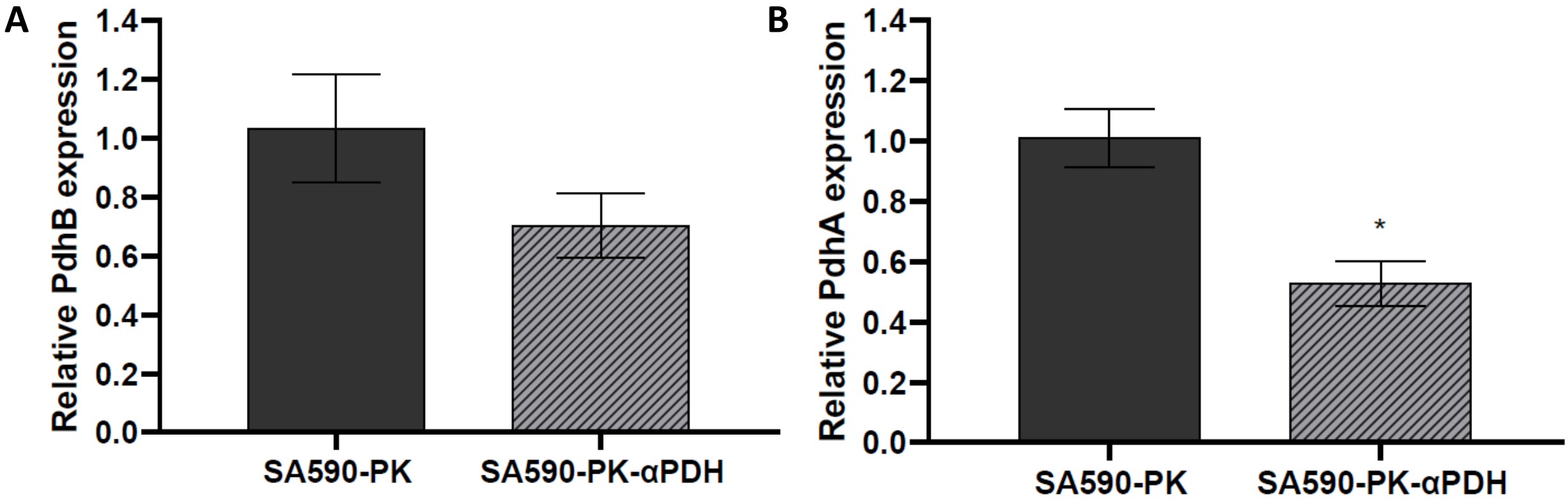
A
Relative PdhB expression
1.4
1.2
1.0
0.8
0.6
0.4
0.2
0.0
SA590-PK
SA590-PK-αPDH
B
Relative PdhA expression
1.4
1.2
1.0
0.8
0.6
0.4
0.2
0.0
*
SA590-PK
SA590-PK-αPDH

Fig. S5

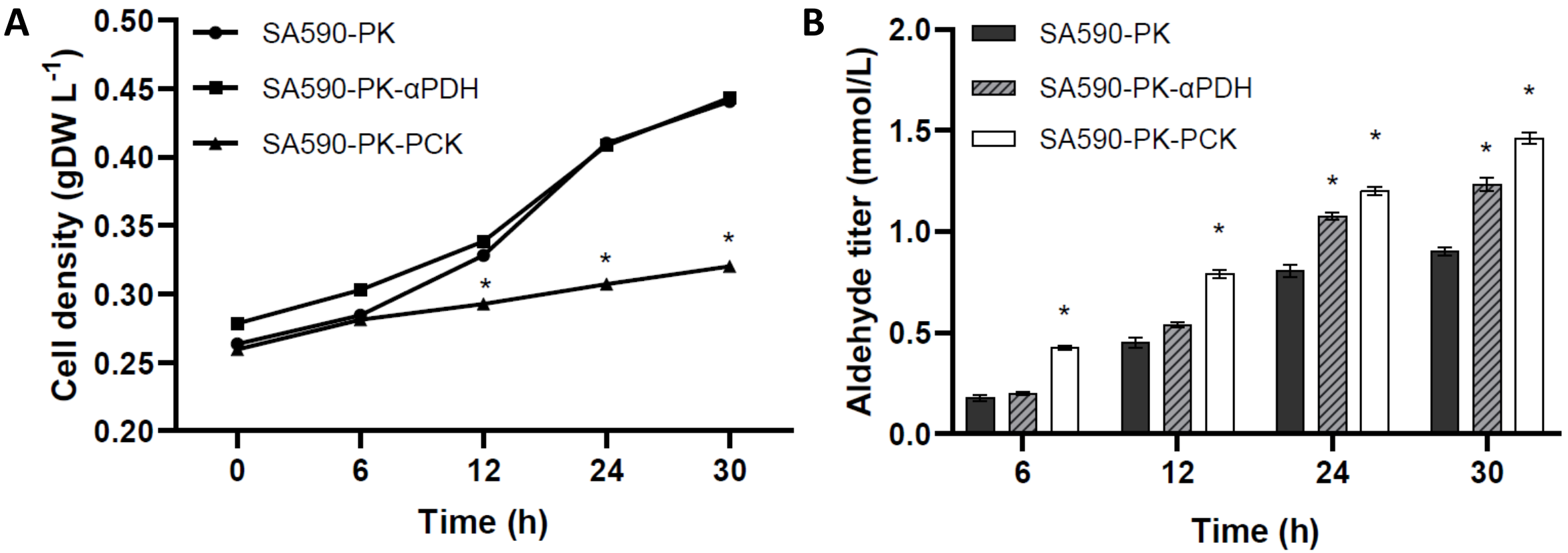
A
Cell density (gDW L-1)
0.50
0.45
0.40
0.35
0.30
0.25
0.20
SA590-PK
SA590-PK-αPDH
SA590-PK-PCK
0
6
12
24
30
Time (h)
B
Aldehyde titer (mmol/L)
2.0
1.5
1.0
0.5
0.0
SA590-PK
SA590-PK-αPDH
SA590-PK-PCK
6
12
24
30
Time (h)

Fig. S6

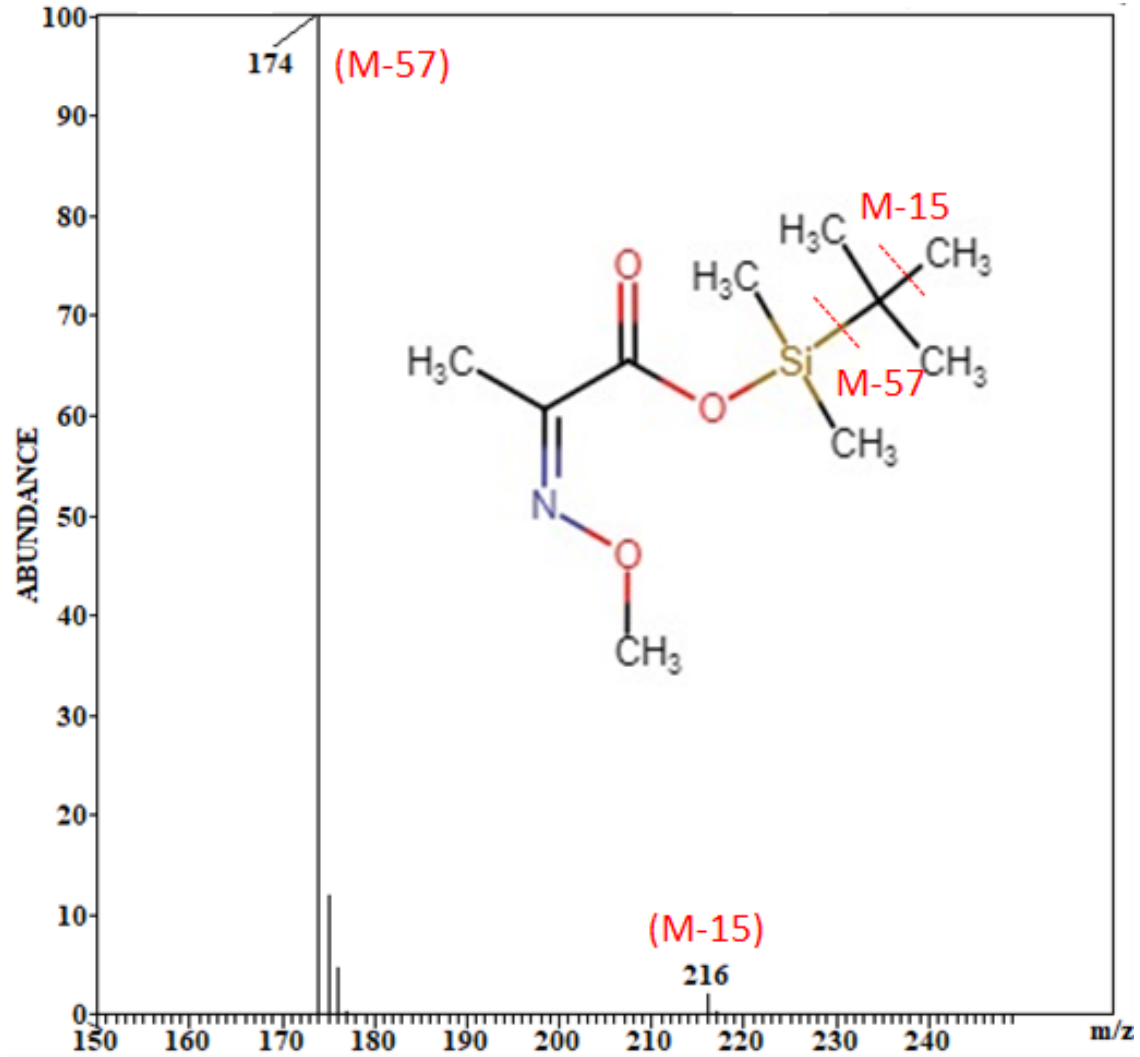
ABUNDANCE
100
90
80
70
60
50
40
30
20
10
0
150
160
170
180
190
200
210
220
230
240
m/z
174
(M-57)
216
(M-15)
M-15
M-57
O
N
Si
H_3C
CH_3

Fig. S7

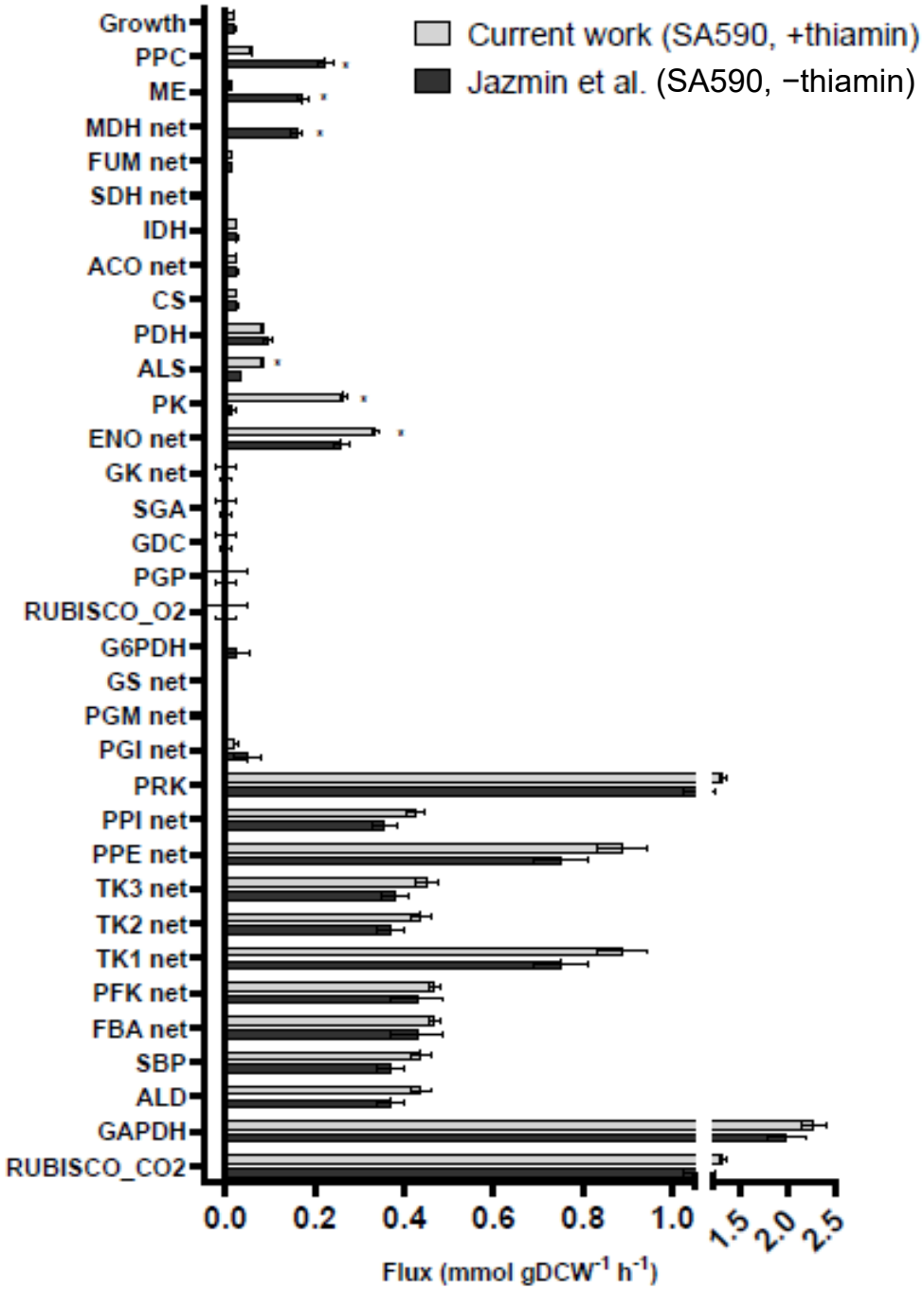
Current work (SA590, +thiamin)
Jazmin et al. (SA590, −thiamin)
Growth
PPC
ME
MDH net
FUM net
SDH net
IDH
ACO net
CS
PDH
ALS
PK
ENO net
GK net
SGA
GDC
PGP
RUBISCO_O2
G6PDH
GS net
PGM net
PGI net
PRK
PPI net
PPE net
TK3 net
TK2 net
TK1 net
PFK net
FBA net
SBP
ALD
GAPDH
RUBISCO_CO2
0.0
0.2
0.4
0.6
0.8
1.0
1.5
2.0
2.5
Flux (mmol gDCW^{-1} h^{-1})

Fig. S8

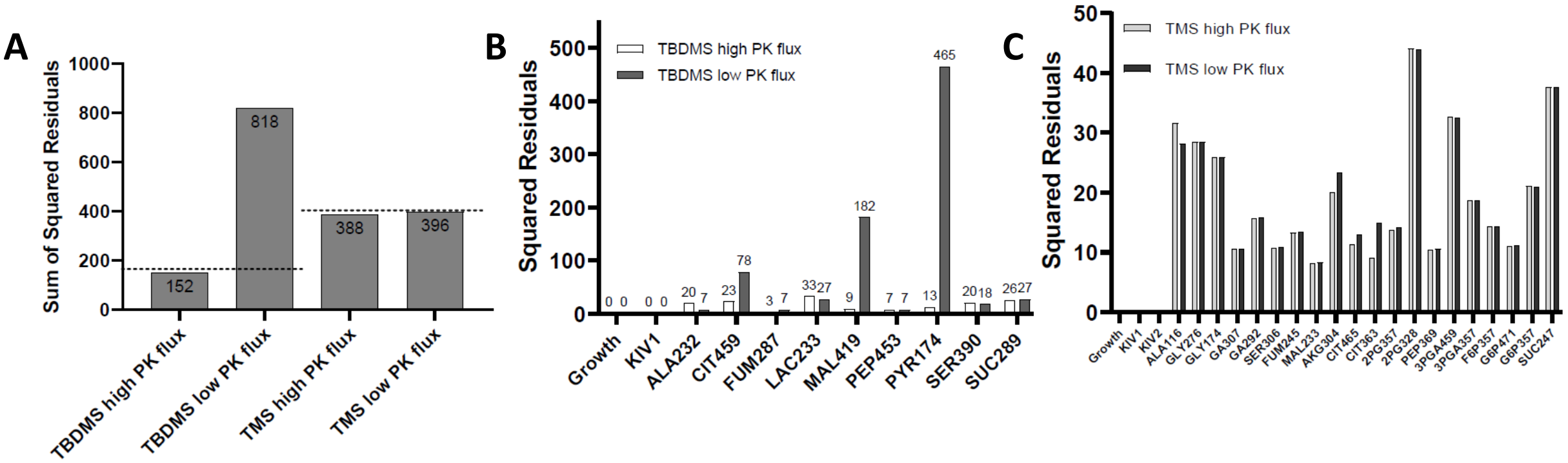
A
Sum of Squared Residuals
1000
800
600
400
200
0
152
818
388
396
TBDMS high PK flux
TBDMS low PK flux
TMS high PK flux
TMS low PK flux
B
Squared Residuals
500
400
300
200
100
0
TBDMS high PK flux
TBDMS low PK flux
0 0
0 0
20 7
23
78
3 7
33 27
9
182
7 7
13
465
20 18
26 27
Growth
KIV1
ALA232
CIT459
FUM287
LAC233
MAL419
PEP453
PYR174
SER390
SUC289
C
Squared Residuals
50
40
30
20
10
0
TMS high PK flux
TMS low PK flux
Growth
KIV1
KIV2
ALA116
GLY276
GLY174
GA307
GA292
SER306
FUM245
MAL233
AKG304
CIT465
CIT363
2PG357
2PG328
PEP369
3PGA459
3PGA357
F6P357
G6P471
G6P357
SUC247